2 Background Theory

The derivation of MOST relies on several crucial and limiting assumptions. First, MOST is only valid within a well-defined surface layer where turbulent fluxes vary by no more than 10% with height (Stull, 1988). This is often not the case for sloping terrain (Nadeau et al., 2013), nocturnal conditions (Mahrt, 1999) and transient processes (Cheng et al., 2005; Lothon and Lenschow, 2011). Second, the terrain is flat and homogeneous. Finally, the flow is quasi-stationary, meaning the turbulence statistics are unaffected by temporal translations of the averaging period. Given these assumptions, dimensional analysis is used to define a single, non-dimensional length scale,

$$\zeta = \frac{z - d_0}{L}, \tag{1}$$

where z is the height above the surface, d_0 is the displacement height, which is assumed to be zero at both sites, and L is the Obukhov Length, defined as

$$L = \frac{-u_*^3}{\kappa \frac{g}{\overline{\theta_0}} \overline{w'\theta_0'}} \tag{2}$$

where u_* is the friction velocity, $\overline{\theta_0}$ is the absolute mean air potential temperature at the surface, $\kappa = 0.4$ is the von Kármán constant, g is acceleration due to gravity and $\overline{w'\theta_0'}$ is the surface kinematic heat flux.

Within the MOST framework, the non-dimensionalized temperature (ϕ_h) and wind speed (ϕ_m) gradients are unknown functions of only ζ:

$$\frac{\kappa z}{\theta_*}\frac{\partial \overline{\theta}}{\partial z} = \phi_h(\zeta), \tag{3}$$

and

$$\frac{\kappa z}{u_*}\frac{\partial \overline{U}}{\partial z} = \phi_m(\zeta), \tag{4}$$

where $\overline{\theta}$ and $\overline{U}$ are the mean potential temperature and wind speed and $\theta_* = -\overline{w'\theta_0'}/u_*$, is a scaling temperature.

The form of ϕ_m and ϕ_h is most commonly determined empirically. Here we use the formulations recommended by Dyer (1974):

$$\phi_h = \phi_m^2 = (1 - 16\zeta)^{-0.5} \text{ for } \zeta < 0, \tag{5}$$

$$\phi_h = \phi_m = 1 + 5\zeta \text{ for } \zeta \geq 0. \tag{6}$$

From the definition of ϕ_h and ϕ_m, the eddy viscosities of heat (K_h) and momentum (K_m) can be determined from:

$$K_h = \kappa z \theta_* / \phi_h(\zeta), \tag{7}$$

$$K_m = \kappa z u_* / \phi_m(\zeta). \tag{8}$$

For the lowest model level, K_h and K_m are always assumed to be positive. Thus, for the near surface, the turbulent fluxes are assumed to always be proportional to the negative local gradient.

3 Methods

Data for the analysis were collected during the Mountain Terrain Atmospheric Modeling and Observations Program. The principal objective of MATERHORN is to improve weather predictability in regions of complex terrain. The experimental portion of the program consisted of two field campaigns that took place at the United States Army Facility, Dugway Proving Ground in Utah's West Desert, USA. The first field campaign ran from 26 September – 7 November 2012 and focused on quiescent conditions with minimal synoptic forcing. The second campaign ran from 1 May – 6 June 2013 with an emphasis on synoptically-driven flows. Through both campaigns, meteorological towers, radiometers, and soil sensors ran continuously with additional instrumentation deployments such as tethered and free flying balloons, aircraft, lidars, hot wire anemometers, and infrared cameras during 24 hour intensive observation periods (IOPs). The fall campaign consisted of nine IOPs while the spring campaign consisted of ten. Full details and objectives of the MATERHORN program are found in (Fernando et al., submitted to *Bull. Amer. Meteor. Soc.*).

3.1 Experimental Sites and Instrumentation

For the current study, we consider two highly instrumented sites. First, the Playa site is located on a large desert playa with no vegetation and an elevation of 1296 m above sea level (40°8'5.9" N, 113°27'7.8" W). The mean soil and surface characteristics for both sites are reported in Table 1. The playa surface and soil characteristics are nearly homogeneous following a rain event with a gradual increase in spatial heterogeneity until another rain event occurs. Due to high soil salinity at the Playa site, the volumetric water content (*VWC*) measurements were made by hand. The fall measurements were conducted only three times at a single location while the spring measurements were conducted every IOP at 20 locations (Hang et al., submitted to *Bounda.-Layer Meteor.*). Thus a direct comparison between the fall and spring *VWC* is impossible. Based on the surface albedo (a), thermal conductivity (k) and volumetric heat capacity (*VHC*) it is evident the mean soil moisture at the Playa was higher during the fall campaign than the spring. Under quiescent, convective conditions, an up-valley northerly flow develops. There is a typical calm period associated with sunset followed by the development of a down-valley southerly flow with a jet-like structure through much of the night.

The Sagebrush site is located approximately 25 km to the east of the Playa site (40°7'16.9" N, 113°7'44.7" W) at an elevation of 1316 m above sea level. The two sites are separated by Granite Peak, a small mountain with a maximum elevation of 840 m above the valley floor (Fig. 1). The vegetation is predominately Greasewood (Emrick and Hill, 1999) on the order of 1 m tall. The *VWC* is much lower at the

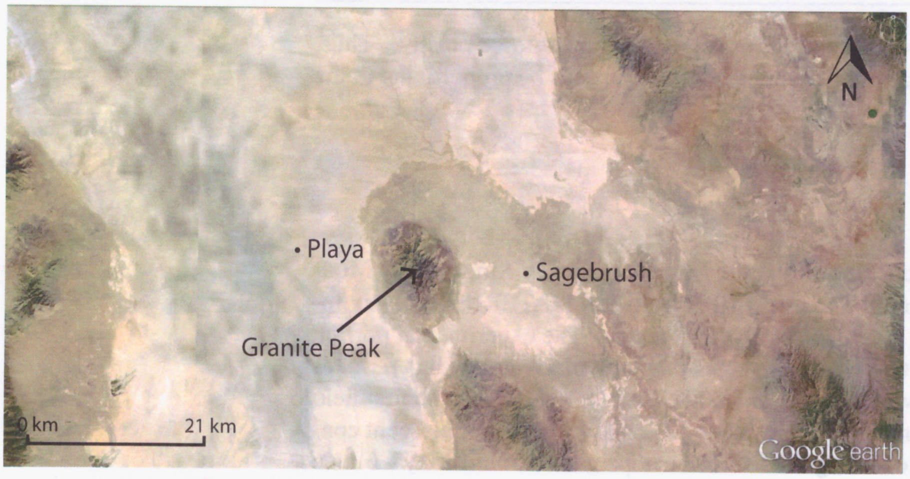

Fig. 1 Map of the two experimental sites (Google Earth, 2013).

Sagebrush site, allowing for a smaller VHC and thermal inertia (TI). Contrary to the Playa site, the mean soil moisture at Sagebrush is higher during the spring campaign. Additionally the leaf area index (LAI) increases and subsequently decreases the mean surface albedo. Under quiescent, daytime conditions a north-westerly breeze develops; following the calm associated with transition, a southerly drainage flow develops with the formation of occasional low-level jets.

Table 1 Soil and surface characteristics at the Playa and Sagebrush sites. VWC is the volumetric water content, a is the surface albedo, k is the 50 mm thermal conductivity of the soil, VHC is the 50 mm volumetric heat capacity, TI is the 50 mm thermal inertia of the soil computed from $TI \equiv (k * VHC)^{0.5}$, LAI is the leaf area index estimated from NASA's MODIS tool, and z_0 is the surface roughness (Sect 3.2).

	Site	VWC	a	k (W m^{-1} K^{-1})	VHC (MJ K^{-1} m^{-3})	TI (J m^{-2} K^{-1} s$^{-1/2}$)	LAI	z_0 (mm)
Fall	Playa	0.30	0.31	0.90	2.2	1400	0	0.61
	Sagebrush	0.09	0.27	0.49	1.3	800	0.17	93
Spring	Playa	0.38	0.33	0.77	2.1	1270	0	0.11
	Sagebrush	0.13	0.24	0.72	1.7	1100	0.24	140

At both sites, sonic anemometers and fine-wire thermocouples were used to capture turbulence data at multiple levels. The fine-wire thermocouples used were 0.0127 mm in diameter with no radiation shield or active ventilation as the solar loading is expected to be negligible (Erell et al., 2005). The thermocouples were placed near the centre of sonic path for a spatial separation on the order of several tens of millimeters. The Playa site had six measurement levels between 0.5 and 26 m, while the Sagebrush site had five measurement levels between 0.5 and 20 m. Due to occasional instrumentation problems at the 26-m Playa tower, and to create consistency between sites, we only examine the five measurement heights between 0.5 and 20 m at both sites. Fast-response, open-path, infrared gas analyzers were positioned at 10 m at both sites, with a spatial distance of 60 mm from the sonic anemometer measurement volume, to measure fluxes of moisture (H_L) and CO_2 (H_{CO2}). Ground heat flux (H_G) was calculated from measurements of the subsurface heat flux at 50 mm depth and the change in heat storage between the flux plates and the surface. Two self-calibrating heat flux plates were buried approximately 50 m to the west of the towers. The soil heat storage above the flux plates was calculated from soil temperature measurements at 10, 25, and 50 mm, and the volumetric heat capacity was measured with a thermal property sensor. Finally, the four components of the radiation balance were measured on a sawhorse-type structure at 2 m above the surface. Site and sensor information is given in Table 2 and Fig. 2.

Table 2 Instrumentation deployed at the Playa and Sagebrush sites. Accuracy given as reported by the manufacturer. Tower locations refer to Fig. 2. u, v, and w are the streamwise, spanwise and vertical velocity components, respectively; T_s is the sonic derived temperature; H_2O and CO_2 are the mass densities of H_2O and CO_2; P is atmospheric pressure; T is air temperature; RH is relative humidity; T_G is ground temperature; k is the soil thermal conductivity and α is the soil thermal diffusivity.

Instrument name	Variables measured	Accuracy	Sample frequency (Hz)	Manufacturer	Tower Locations
CSAT3	u, v	± 0.08 m s^{-1}	20	Campbell Sci.	A, B, C, D,
	w	± 0.04 m s^{-1}			E, F, J
	T_s	n/a			
EC150	H_2O	n/a	20	Campbell Sci.	D, J
	CO_2	n/a			
	P	± 15 hPa			
RMY8100	u, v, w	± 0.05 m s^{-1}	20	R.M. Young	G, H, I, K
	T_s	$\pm$ 2°C			
FW05	T	± 0.07°C	20	Campbell Sci.	All
HMP45	T	± 0.25°C	1	Vaisala	All
	RH	$\pm$ 2%			
HFP01SC	H_G	± 3% of reading	1/600	Hukseflux	−50 mm
HTTC36 T-18G-6	T_G	n/a	1/600	Omega Eng.	−10, −25, −50 mm
TP01	k	± 5%	1/600	Hukseflux	− 50 mm
	α	± 20%			

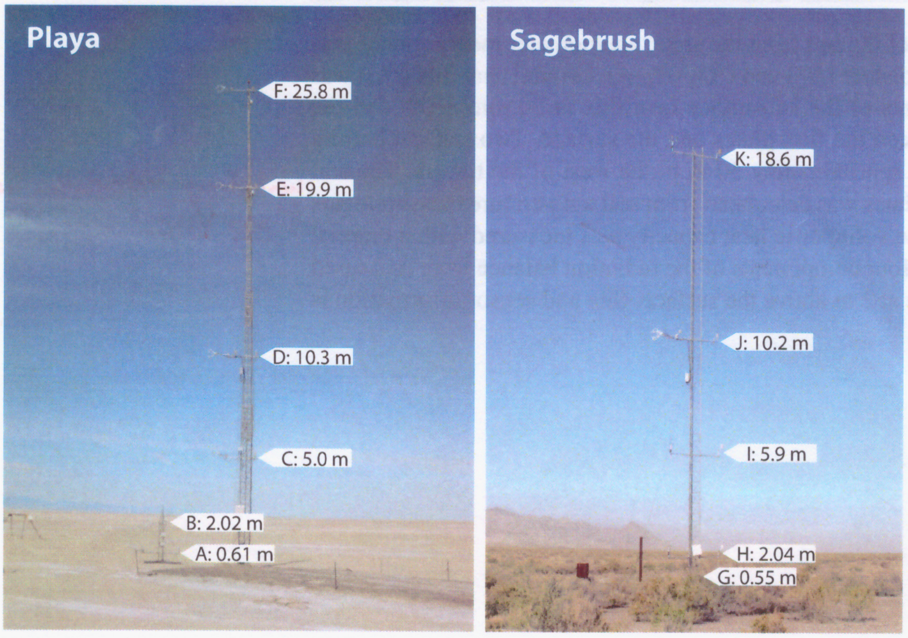

Fig. 2 Photographs looking north-west toward the Playa tower (left) and Sagebrush tower (right) with instrument heights imposed on the image. The northern portion of Granite Peak is visible behind the Sagebrush tower. Height labels refer to Table 2. For simplicity, tower heights are referred to as 0.5, 2, 5, 10, 20, and 26 m throughout this study. The 0.5 and 2 m Playa instrumentation is mounted on a smaller tower to the west of the main tower to minimize flow distortion. At both sites there is a solar sawhorse and soil sensors approximately 50 m to the west of the tower to measure net radiation and ground heat flux (sawhorse not pictured at the Sagebrush site).

At both sites, the radiation balance and ground heat flux observations are made 50m ...

3.2 Surface Roughness

The surface roughness parameter (z_0) was estimated by considering wind speed profiles where $|L_{10\ m}| > 100$. At the Sagebrush site, the 0.5 m measurement was removed because it was located within the vegetative canopy. At the Playa site, only profiles where the 10-m wind direction was greater than 300° and less than 40° were considered. This was done to avoid flow distortions associated with a nearby road and storage container. Next, a least squares, linear fit was calculated with the wind speed (U) and $\ln(z)$, yielding a slope (m) and intercept (b). Cases where the R^2 value of the fit fell below 0.99 were removed. z_0 was then found for each profile with $\tilde{z}_0 \approx e^b$. Finally, the median value of $\tilde{z}_0$ was used to estimate z_0.

...linear fit for the wind speed (u) as function of ln(z) ...

Table 1 gives results for the fall and spring campaigns. As expected, $z_{0,Playa} \ll z_{0,Sagebrush}$. At Playa, z_0 is larger during the fall due to cracks in the soil surface. In the spring, the cracks are much smoother creating a quasi-smooth surface. z_0 at the Sagebrush site is larger during the spring campaign due to increased vegetation, which is consistent with the observed LAIs.

3.3 Data Analysis

Data were analyzed with the Utah Turbulence in Environmental Studies processing and analysis code (UTESpac). Despiking and quality control were performed following Vickers and Mahrt (1997), planar fitting was applied following Wilczak et al. (2001) and density corrections were applied to the latent heat flux following Webb et al. (1980). Based on the previous work of Blay-Carreras et al. (2014) and ogive tests (Aubinet et al., 2012), 5-min averaging periods were used for linear detrending of the data as well as flux calculations. The nocturnal energy balance nearly closes with this methodology, with residuals on the order 10 W m^{-2} at both sites. Under daytime conditions the residual is significantly larger, with a peak magnitude of approximately 100 W m^{-2} at both sites. The large daytime residual is likely due to two things. First, the 5-min averaging likely misses some of the flux associated with large, daytime eddies. Second, linear detrending effectively high pass filters the data (Finnigan et al., 2003; Aubinet et al., 2012), which further removes energy associated with the large scales. Nevertheless, due to the rapidly evolving conditions through the LAEET, 5 min averaging with linear detrending is chosen as the best combination to isolate the turbulent motions through the LAEET. Finally, due to the spectral uncertainty through the LAEET and small spatial separations in the eddy-covariance systems, no spectral corrections were applied (Aubinet et al., 2012).

Temperature gradients were computed from the fine-wire thermocouples using finite difference techniques. A forward difference is used for the lowest level (Error $O(dz)$), a backward difference for the highest level (Error $O(dz)$), and a three-point difference (Error $O(dz^2)$), utilizing the analytical derivative of a Lagrange interpolating polynomial, for the middle levels (Chapra and Canale, 2010).

3.4 Transition Analysis

In order to study flux-gradient relationships through the LAEET, a relative time τ is defined as $\tau = t - t_{Rn=0}$ where t is time and $t_{Rn=0}$ is the first time period when the local net radiation has gone below 0. τ_{flux} represents the relative time when the sensible heat flux (H) crosses 0 and τ_{grad} represents the relative time when the potential temperature gradient ($\partial\overline{\theta}/\partial z$) crosses 0. In an effort to reduce ambiguity, the identification method of τ_{grad} and τ_{flux} differ one from the other. τ_{grad} is defined as the timestep following the last period where the gradient was less than 0. This is because the gradients at 5 m and above frequently display quasi-neutral behaviour with weakly positive and negative values before stabilization occurs. Once the stabilization has occurred the gradients typically become persistently positive. Contrarily, τ_{flux} is identified by the first time period where the heat flux becomes negative. This is because the strongly positive fluxes transition into weakly negative fluxes with occasional positive values. The reversals were identified computationally with careful examination to ensure that the reversal is accurately captured. The mean gradient and heat flux behaviour is addressed in Sect. 4.3 and 4.4, respectively.

Next, We define a time lag, $t_{lag} = \tau_H - \tau_{grad}$ to quantify delays between the gradient and flux reversals. Therefore, $t_{lag} > 0$ indicates the gradient reversal precedes the flux reversal and $t_{lag} < 0$ indicates the flux reversal precedes the gradient reversal (The behavior observed by Blay-Carreras et al. (2014)).

Finally, we filter the data to eliminate transitions with incomplete data availability, excessive clouds, mean wind speeds above 10 m s^{-1} at 5 m, and non–monotonically increasing temperatures at the beginning of the late afternoon transition. We do this to limit our study to idealized, quiescent days with little synoptic forcing in an effort to focus on microscale phenomena. We are left with 8 transition periods at Playa and 13 at Sagebrush.

4 Results and Discussion

4.1 Surface Fluxes

Fig. 3 shows the averaged net radiation (R_n), sensible heat flux (H) and latent heat flux (H_L) for the fall campaign at both sites. Despite the higher albedo at Playa, the daytime R_n is quite similar at both sites with a slightly more rapid development and decay at the Playa site, which is due to the higher TI of the playa soil. Under nighttime conditions, $|R_n|$ is significantly higher at the Playa site due to the much higher VHC. For similar reasons, H at the Playa site develops and decays more slowly, with maximum daytime values approximately 30 W m^{-2} less than those of Sagebrush. The nighttime values of H at Playa are very weak, indicating a near balance between the ground heat flux (H_G) and R_n.

Given the arid nature of the region, the magnitude of H_L is quite small at both sites, with daytime values of H_L being slightly smaller at the Playa site. This indicates that the shallow crust on the surface of the playa is effective at preventing the transport of latent heat and vegetative transpiration at the Sagebrush site may represent a significant portion of the moisture transport budget. The daytime Bowen ratio, defined as $BR \equiv H/H_L$, is approximately 8 at both sites.

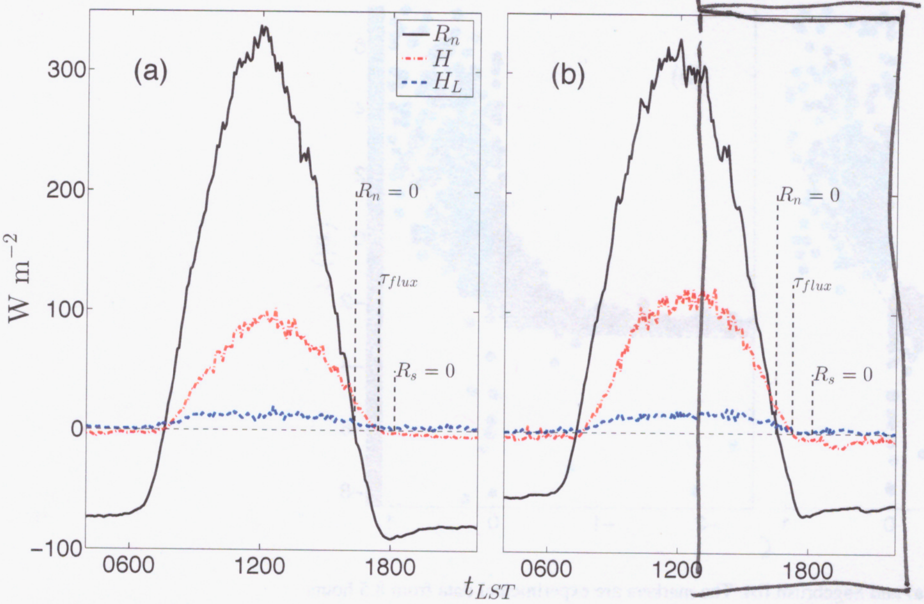

Fig. 3 The averaged diurnal cycle of the net radiation (R_n), sensible heat flux (H) and latent heat flux (H_L) at 10 m averaged over the fall campaign for the Playa **(a)** and Sagebrush **(b)** sites.

4.2 Monin-Obukhov Scaling and Counter-Gradient behaviour

The non-dimensional temperature gradient (ϕ_h) is plotted vs stability (ζ) in Fig. 4. For moderately unstable conditions ($-2.5 < \zeta \lesssim -0.2$), both sites scale quite well and ϕ_h is only slightly larger than the Dyer and Hicks (1970) formulation (Eq. 5). For moderately stable conditions ($0.2 \lesssim \zeta < 1$), the scatter is large at both sites. There is a trend but it is much noisier and the slope is much steeper than Eq. 6 predicts, suggesting that an alternate formulation of ϕ_h may be more appropriate. Under near-neutral conditions ($-0.1 \lesssim \zeta \lesssim 0.1$), there is an asymptotic behaviour with large positive and negative values. This behaviour is due to H showing up in the denominator of ϕ_h via θ_*(Eq. 7). As H passes through 0, extreme values of ϕ_h occur. Theoretically, this regime corresponds to the classical neutrally stratified surface layer where H is no longer a relevant scaling parameter. However, neutral scaling does not apply during this transition either. For $\phi_h \gg 0$, MOST is invalid but the behaviour is not CG. For $\phi_h \ll 0$, MOST is invalid and the heat flux is CG. Most transitions are characterized by an approximately equal number of highly positive and highly negative number of data points. This indicates, to a first order approximation, MOST is expected to fail for roughly two times the CG duration.

Table 3 CG information for 2 m at Playa and Sagebrush. In general, $t_{Rn=0}$ occurs 10-20 min earlier at Sagebrush. t_{lag} is computed by subtracting τ_{grad} from τ_{flux}.

Site	Date	τ_{grad} (min)	τ_{flux} (min)	t_{lag} (min)
Playa	7 Oct '12	45	65	20
	14 Oct '12	35	40	5
	15 Oct '12	10	20	10
	17 Oct '12	60	70	10
	18 Oct '12	55	70	15
	19 Oct '12	10	20	10
	20 Oct '12	−25	0	25
	21 Oct '12	45	70	25
Sagebrush	28 Sept '12	40	30	−10
	29 Sept '12	20	15	−5
	1 Oct '12	45	30	−15
	2 Oct '12	25	20	−5
	3 Oct '12	30	20	−10
	4 Oct '12	30	25	−5
	6 Oct '12	45	35	−10
	7 Oct '12	45	40	−5
	8 Oct '12	25	35	10
	9 Oct '12	20	15	−5
	12 May '13	20	15	−5
	24 May '13	30	20	−10
	30 May '13	20	20	0

Box plots are used to illustrate τ_{grad}, τ_{flux} and t_{lag} for all heights across all days considered (Fig. 6 - 8). Beginning with τ_{grad}, the 2-m behaviour discussed above is consistent with the behaviour at the other heights. The variability is smaller at Sagebrush and the median value is approximately constant between sites for a given height. Furthermore, gradient reversal appears to be a top-down phenomena with a slope of

$$\frac{\partial \tau_{grad}}{\partial z} \approx -4 \text{ min m}^{-1} \qquad (9)$$

at both sites. Indicating that within the context of this study, gradient reversal is site independent.

Eq. 10 generally captures the trend and typically falls within the interquartile range (IQR) of the box plots (marked by the limits of the the box).

4.3 Temperature Gradient Evolution and Flux Divergence

To understand the differing CG behaviour at the Playa and Sagebrush site, the temperature gradient and heat flux evolution are considered independently. First, the temperature gradient evolution is discussed followed by the heat flux evolution in Sect. 4.4.

The ensemble temperature gradient evolution is shown for both sites in Fig. 9. As expected, the relative strength of the gradients is much stronger at Sagebrush for both before and after $\tau = 0$. The gradients at 10 and 20 m at Sagebrush are quasi-neutral and slowly begin to stabilize around $\tau = 0$. This is also the case at the Playa site but at Playa, the 5-m gradient is also quasi-neutral before stabilization occurs. At both sites, the weak gradients aloft cross 0 before the stronger, near-surface gradients at 0.5 and 2 m. Additionally, there is never a period where all of the gradients are near-neutral. In fact, at both sites there appears to be a convergence zone where all of the gradients are approximately equal and weakly stable. This abrupt transition through 0 supports the modeling work of Jiménez et al. (2012) and observations of Acevedo and Fitzjarrald (2001) where the transition through neutral stratification happens abruptly.

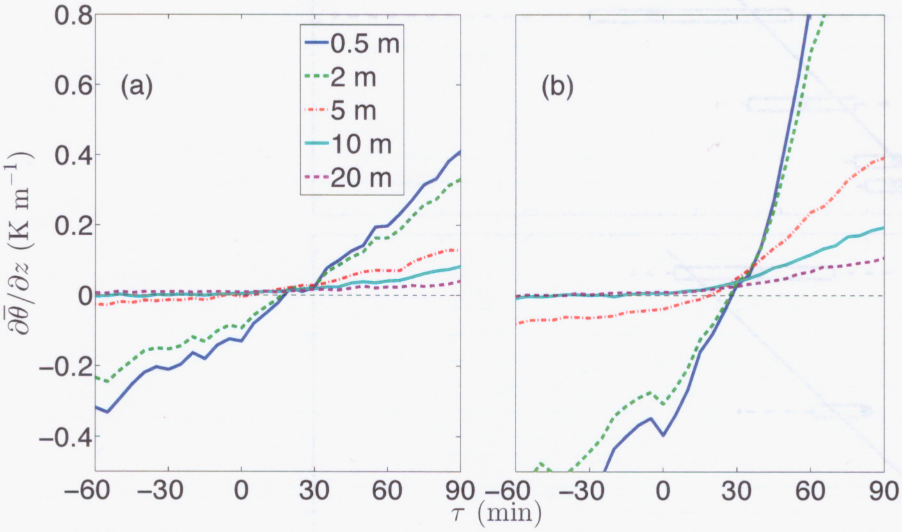

Fig. 9 Ensembled potential temperature gradient for all heights at the Playa (**a**) and Sagebrush sites (**b**).

The weak gradients aloft help to explain why the gradient reversal occurs from the top down. Temperature tendency profiles are shown in Fig. 10. Once again, the magnitude of the cooling at Sagebrush is much larger than that of Playa. At both sites the cooling is largest and initiated near the ground. The stabilization in the layer is proportional to the slope of the temperature tendency profile. Therefore, while stabilization is occurring most rapidly near the surface, the very weak gradients aloft are able to flip with a very small amount of stabilization, creating the observed top-down behavior.

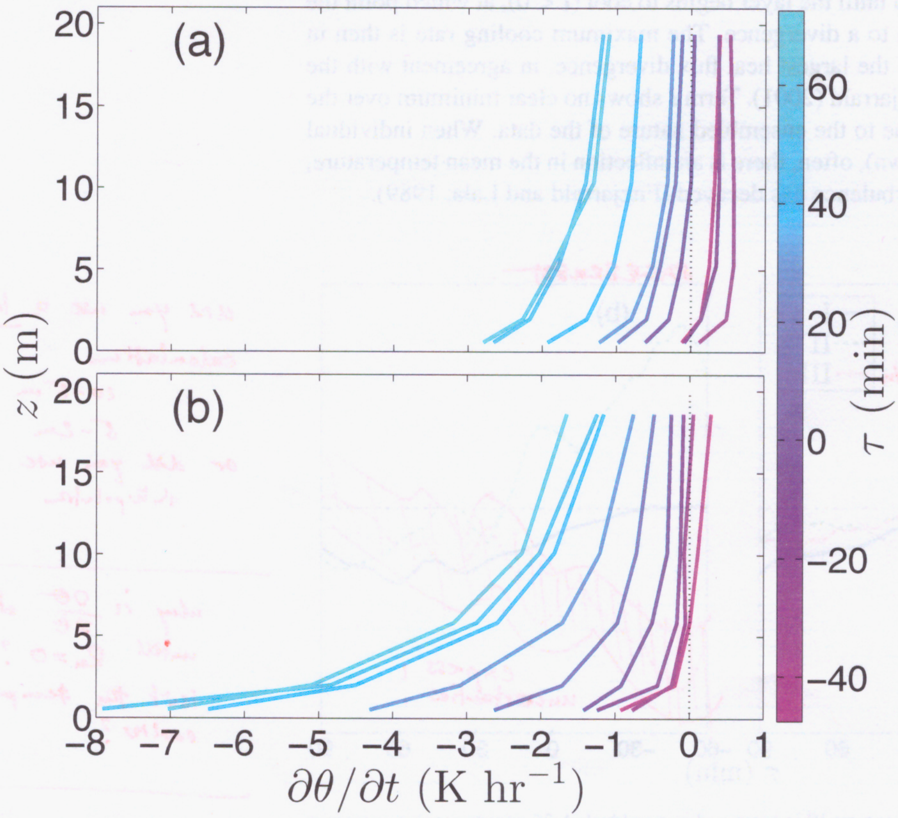

Fig. 10 Profiles of $\partial\overline{\theta}/\partial t$ at Playa **(a)** and Sagebrush **(b)**. To the right of the dashed line, heating is occurring and to the left of the dashed line, cooling is. A 15 minute bin-average was applied to the profiles.

To understand where the cooling is coming from, the simplified temperature tendency equation is considered:

$$\underbrace{\frac{\partial\overline{\theta}}{\partial t}}_{\text{I}} = \underbrace{-\frac{\partial\overline{w'\theta'}}{\partial z}}_{\text{II}} \underbrace{+ADV_\theta - \frac{\partial R_n}{\partial_z}}_{\text{III}} \tag{11}$$

where term I is the temperature storage, II is the sensible heat flux divergence, and III, which is computed as the residual, is the sum of all advective effects (ADV_θ) and the radiative flux divergence($\frac{\partial R_n}{\partial_z}$). It is expected that early in the LAEET, ADV_θ will be relatively small and gradually increase in importance as the size of the mixing eddies decreases and surface heterogeneities are amplified (Acevedo and Fitzjarrald, 2001, 2003).

The terms of Eq. 11 are plotted at 5 m for both sites in Fig. 11. When terms *II* or *III* are greater than 0, the term is warming the layer; when they are less than zero, the term is cooling the layer. Starting at the Playa site, *II* begins to cool the layer at approximately the same time *I* becomes negative. That is, there is a heat flux convergence in the layer until until the layer begins to cool ($I < 0$), at which point the convergence gradually shifts to a divergence. The maximum cooling rate is then in approximate agreement with the largest heat flux divergence, in agreement with the findings of Acevedo and Fitzjarrald (2001). Term *I* shows no clear minimum over the time range shown. This is due to the ensembled nature of the data. When individual days are considered (not shown), often, there is an inflection in the mean temperature, indicating the mechanical turbulence has decayed (Fitzjarrald and Lala, 1989).

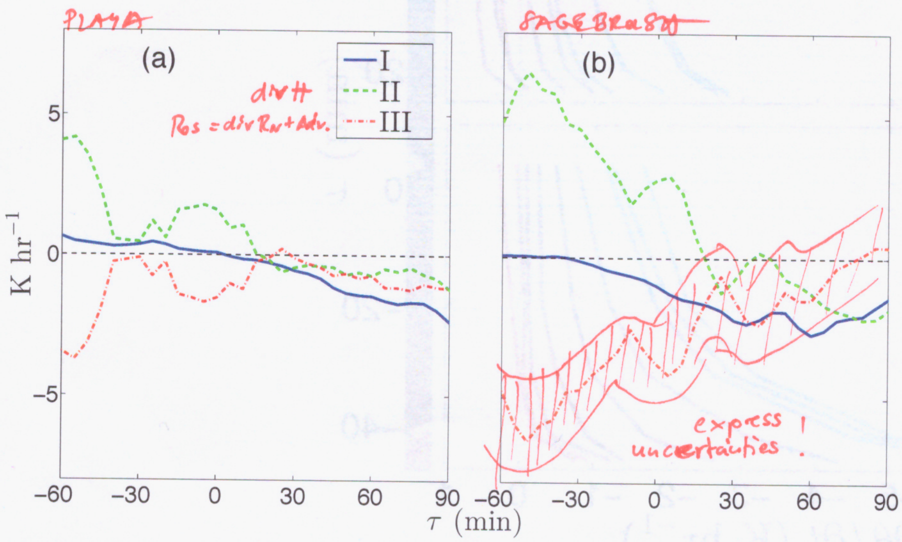

Fig. 11 Terms of Eq. 11 at 5 m where term III is computed as a residual. A 25 minute running average is used to smooth the ensembled data

At the Sagebrush site, *I* becomes negative significantly earlier than *II*, with the maximum cooling rate occurring in the presence of a weak heat flux convergence. This is counter to the findings of Acevedo and Fitzjarrald (2001), where the maximum cooling rate was found to coincide with the maximum heat flux divergence. Furthermore, the magnitudes of *I* and *II* differ significantly for both sites. Considering the relative homogeneity of both sites, it appears that radiative flux divergence becomes important early in the LAEET and should not be neglected in models. When other tower heights are considered (not shown), the observed behaviour is very similar to the 5-m level, the only difference being that the relative magnitude of the terms decreases with height.

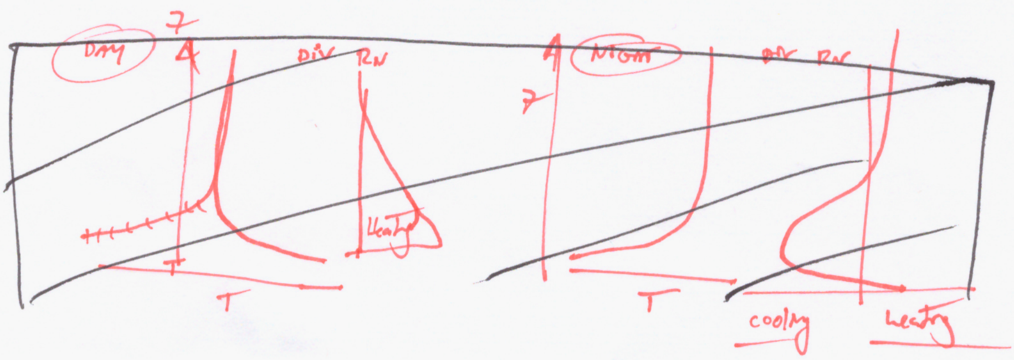

4.4 Heat Flux Evolution

Here, the sensible heat flux evolution is considered. The ensembled sensible heat flux evolution is shown in Fig. 12. Beginning at the Playa site, the decay is gradual with a small amount of variability (heat flux convergence) between levels. All levels cross 0 at approximately the same time and a weak heat flux divergence gradually develops through the evening transition. At the Sagebrush site, the decay is much more abrupt, with a large heat flux convergence occurring in the lower levels. The levels above 0.5 m cross 0 at approximately the same time with the 0.5-m flux crossing 5–10 minutes later. This is likely due to shielding from the surrounding vegetation. Later in the evening transition, the negative fluxes at Sagebrush become stronger than those of Playa with a heat flux divergence developing around $\tau = 45$.

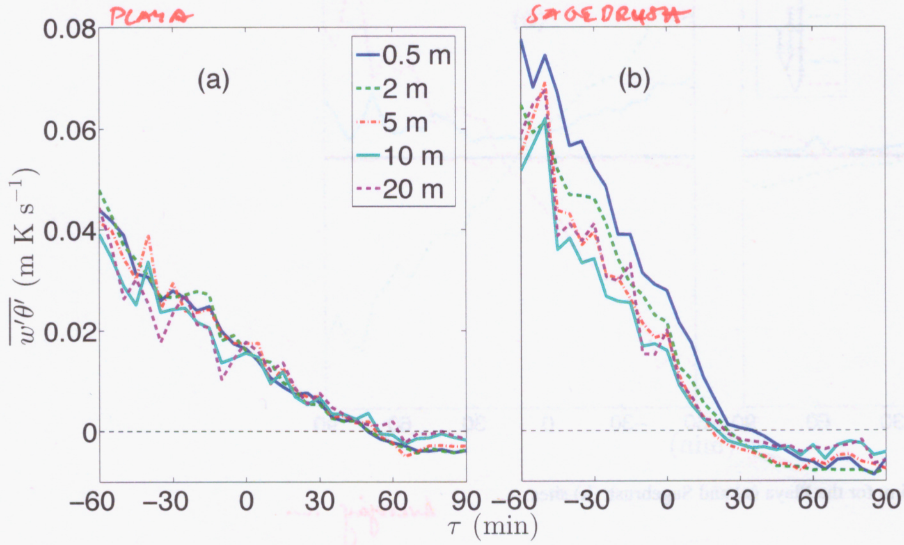

Fig. 12 Ensembled sensible heat flux for all heights at the Playa (**a**) and Sagebrush sites (**b**).

Similar to the temperature gradient evolution, the heat flux evolution is discussed in terms of its simplified tendency equation. Here we used the simplified budget from Wyngaard et al. (1972):

$$\underbrace{\frac{\partial \overline{\theta' w'}}{\partial t}}_{\text{I}} = \underbrace{-\overline{w'^2}\frac{\partial \overline{\theta}}{\partial z}}_{\text{II}} \underbrace{-\frac{\partial (\overline{w'^2\theta'})}{\partial z}}_{\text{III}} \underbrace{+\overline{\theta'^2}\frac{g}{\overline{\theta}}}_{\text{IV}} \underbrace{+\frac{1}{\rho}\overline{\theta'\frac{\partial p'}{\partial z}}}_{\text{V}} \qquad (12)$$

where term *I* is local storage, *II* is gradient production, *III* is the turbulent transport, *IV* is buoyant production and *V* is the pressure destruction. Subsidence, advection, and molecular dissipation are assumed to be small. Terms *I* – *IV* are computed directly and term *V* is computed as a residual. The ensembled terms at 5 m are shown in Fig. 13. Again, the relative magnitude of the terms is much larger at the Sagebrush